Photocurrents in Weyl semimetals

Ching-Kit Chan, Netanel H. Lindner, Gil Refael, and Patrick A. Lee

Phys. Rev. B **95**, 041104 — Published 13 January 2017

DOI: 10.1103/PhysRevB.95.041104

Photocurrents in Weyl semimetals

Ching-Kit Chan,[1] Netanel H. Lindner,[2] Gil Refael,[3] and Patrick A. Lee[1]

[1] *Department of Physics, Massachusetts Institute of Technology, Cambridge, MA 02139, USA*
[2] *Physics Department, Technion, 320003 Haifa, Israel*
[3] *Institute of Quantum Information and Matter and Department of Physics, California Institute of Technology, Pasadena, CA 91125, USA*

(Dated: December 27, 2016)

The generation of photocurrent in an ideal two-dimensional Dirac spectrum is symmetry-forbidden. In sharp contrast, we show that three-dimensional Weyl semimetals can generically support significant photocurrents due to the combination of inversion symmetry breaking and finite tilts of the Weyl spectra. Symmetry properties, chirality relations and various dependences of this photovoltaic effect on the system and the light source are explored in details. Our results suggest that noncentrosymmetric Weyl materials can be advantageously applied to room temperature detections of mid- and far-infrared radiations.

PACS numbers: 72.40.+w, 03.65.Vf, 07.57.Kp

Introduction.—Electronic materials with band crossing excitations have recently attracted much interests in condensed matter physics. A 2D Dirac spectrum describes the surface states of 3D topological insulators [1, 2] and bulk excitations of graphene [3]. Their gapless and topological characters have stimulated many electronic applications, one of which is the photovoltaic effect. The linearly crossing dispersions of Dirac systems can absorb photons with, ideally, arbitrarily long wavelength, making them possibly advantageous for infrared (IR) detections. Nevertheless, the generation of photocurrent, defined as the spontaneous production of current without any applied voltage by the exposure to light, has to vanish for an ideal Dirac spectrum in 2D because of the symmetric excitations about the Dirac point [Fig. 1(a)]. In fact, it has been shown that the resultant photocurrent is negligible even if realistic perturbations including band curvatures, warpings and Zeeman couplings are taken into account [4, 5]. So far, the generation of a substantial photocurrent in Dirac systems has to involve external assistances such as couplings to magnetic superlattices [6]. (Similarly, quantum wires require external magnetic fields to create sizeable photocurrents [7]). Producing photocurrents in Dirac materials remains challenging and has been an active research subject [6, 8–13].

In this paper, we propose that Weyl semimetals can generically develop photocurrents without the need of external couplings. Weyl spectrum is the 3D generalizations of the Dirac cone and thereby shares the same advantage of long-wavelength photon absorptions. Unlike Dirac systems, Weyl semimetals necessarily break either time-reversal (TR) symmetry or spatial inversion (I) symmetry, or both. The photocurrent response of a Weyl system differs from the Dirac counterpart in two crucial ways. First, Weyl cones have definite chiralities and always come in a pairs. They can be regarded as topological monopoles or anti-monopoles of the Berry curvature. For an upright Weyl cone [Fig. 1(b)], the absorption of a circularly polarized photon flips the spin, resulting in asymmetric excitations along the drive direction. Yet, the direction of the photocurrent is governed by the chirality and hence, the sum of photocurrents from a Weyl node pair has to vanish identically. On the other hand, a Weyl cone can be tilted [14, 15] because of reduced symmetries. The corresponding photoexcitation is highly asymmetric about the nodal point [Fig. 1(c)]. The consequential photocurrent is controlled by the tilt and the chirality and there is generally no offset between photocurrents unless additional symmetries are imposed. Note that other interesting effects such as gyrotropic magnetic effect [16, 17], photovoltaic chiral

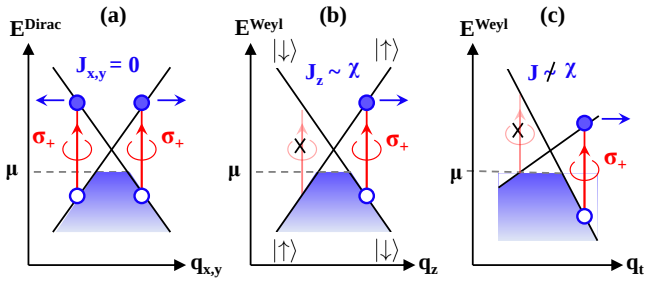

FIG. 1. Schematics of photocurrent generations in Dirac and Weyl systems. Circularly polarized photons propagating along the z-axis induce spin-flip vertical transitions denoted by the red arrows. (a) In an ideal 2D Dirac system, the excitations are symmetric about the node and thus the photocurrent vanishes. (b) In a 3D Weyl system with an upright crossing spectrum, the extra dimension allows an asymmetric particle-hole excitation along q_z and creates a chirality-dependent photocurrent from each Weyl cone. However, the chiral currents from a monopole and an anti-monopole negate each other, yielding no net current. (c) In the presence of tilt along some direction q_t, asymmetric excitations can happen when the system is doped away from the neutrality. The resultant photocurrent is not just determined by the node chirality and the total current is generically non-zero.

magnetic effect [18], anomalous Hall effect [19], emergent electromagnetic induction [20] and nonlinear optical responses [21] can occur in Weyl semimetals, but have different physical origins.

Photocurrents in systems without I symmetry have been observed in semiconductor quantum wells [22] and tellurium [23]. A variety of mechanism has been discussed [23], including real and virtual absorptions and spin-dependent scatterings [22], but the effect is small and the discussion has been limited to quadratic band structures. Here we show that the linear dispersion in Weyl semimetals hold a special advantage and a large photocurrent proportional to the absorption can be produced which survives up to room temperature. In addition to the broken I-symmetry, we find that the presence of finite tilts of the Weyl dispersions, being commonplace in realistic materials, is the key for the photocurrent in Weyl semimetals. The importance of the tilt has not been discussed in the literature so far. The photocurrent response does not require the chemical potential to be tuned to the Weyl point, nor any imbalance of chemical potentials between opposite Weyl nodes, which are otherwise important for chiral-anomaly related responses [18, 24–26]. We investigate the conditions and magnitudes of photocurrents induced by a laser drive and further discuss the potential application for room temperature detections of blackbody IR radiations.

Photocurrent response.—We start by discussing the photocurrents generated from a single Weyl spectrum without any symmetry restriction. The low-energy effective Hamiltonian can be generally written as:

$$H_W(\vec{q}) = \hbar v_t q_t \sigma_0 + \hbar v_F \hat{v}_{i,j} q_i \sigma_j, \tag{1}$$

where v_F is the Fermi velocity without tilt and σ_j are Pauli matrices. $\hat{v}_{i,j}$ represents anisotropy and $\chi = \mathrm{Det}\,(\hat{v}_{i,j}) = \pm 1$ determines the chirality. v_t gives the tilt velocity and $q_t = \hat{t}\cdot\vec{q}$ with $\hat{t}$ being the tilt direction. The linear Weyl dispersion is given by $E_\pm(\vec{q}) = T(\vec{q}) \pm U(\vec{q}) = \hbar v_t q_t \pm \hbar v_F [\sum_j (\sum_i \hat{v}_{i,j} q_i)^2]^{1/2}$ and the ratio v_t/v_F measures the tilt. When $|T(\vec{q})/U(\vec{q})|$ is less than 1 for all $\hat{q}$, the node is in the type-I phase, whereas when it is greater than 1 for some $\hat{q}$, the system is in the type-II regime, in which electron and hole pockets are formed [15].

The interaction with a monochromatic light characterized by $\vec{A}(t) = \vec{A}_+ e^{-i\omega t} + \vec{A}_- e^{i\omega t}$ enters through the Peierls substitution, leading to the interaction Hamiltonian $V(t) = V_+ e^{-i\omega t} + V_- e^{i\omega t}$ with

$$V_\pm = \hbar v_F \hat{v}_{i,j} A_{\pm,i} \sigma_j. \tag{2}$$

$V_{+(-)}$ describes the spin-dependent photon absorption (emission) process. In the isotropic limit $\hat{v}_{i,j} = \delta_{i,j}$, a circularly polarized light propagating along q_z corresponds to $V_\pm = \hbar v_F A \sigma_\pm/2$. We have ignored Zeeman coupling here because the ratio of Zeeman to orbital couplings is $\sim g_s\hbar\omega/(2mv_Fc) \sim 10^{-3}$ [5] based on reported g-factors [27, 28].

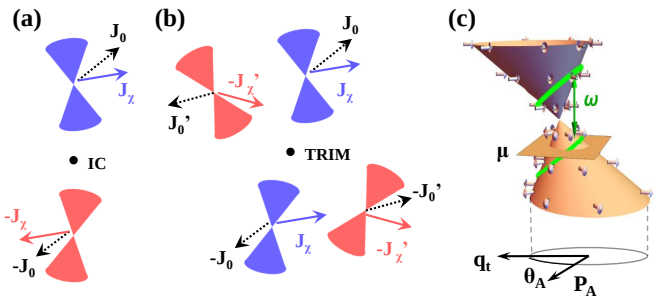

FIG. 2. Relations between photocurrents in centrosymmetric and noncentrosymmetric Weyl semimetals. Each Weyl node produces a photocurrent with chiral-independent ($\vec{J}_0$) and chirality-dependent ($\vec{J}_\chi$) components. (a) In the presence of an inversion center, a pair of I-related Weyl nodes have opposite tilt and opposite chirality, leading to the cancelation of photocurrents. (b) In noncentrosymmetric Weyl systems, TR symmetry relates two Weyl nodes of the same chirality instead. Monopoles and anti-monopoles are not symmetry-related and can have different tilts. Two pairs of Weyl nodes give rise to an overall photocurrent of $2(\vec{J}_\chi - \vec{J}'_\chi)$. (c) defines the angle θ_A between the tilt q_t and Poynting vector P_A.

We now compute the photovoltaic current $\vec{J} = (-e)\sum_{q,l=\pm} [\partial E_l(\vec{q})/\partial\vec{q}] \times [n_l(\vec{q}) - n_l^0(\vec{q})]$, where $n_\pm(\vec{q})$ and $n_\pm^0(\vec{q})$ are the perturbed and equilibrium distribution functions, respectively. Within Fermi's golden rule and the relaxation time approximation, each Weyl node contributes a photocurrent density:

$$J_i = \left(\frac{-e\tau\omega^2 A^2}{16\pi^2}\right) \bar{J}_i, \tag{3}$$

with a dimensionless response function

$$\bar{J}_i(\omega) = 4\int d^3 \left(\frac{v_F q}{\omega}\right) \frac{\partial[\Delta E(\vec{q})/\hbar]}{\partial(v_F q_i)} \left|\left\langle q_+ \left| \frac{V_+}{\hbar v_F A} \right| q_- \right\rangle\right|^2 \times \delta\left(\frac{\Delta E(\vec{q})}{\hbar\omega} - 1\right) [n_-^0(\vec{q}) - n_+^0(\vec{q})], \tag{4}$$

where $\Delta E = E_+ - E_-$. We have introduced a relaxation time τ to account for disorder and phonon scattering [29, 30]. This response function describes the vertical transition from state $|q_-\rangle$ to $|q_+\rangle$ by absorbing a photon with frequency ω. Each particle-hole excitation produces a current $-e\partial[\Delta E(\vec{q})/\hbar]/\partial\vec{q}$ being independent of the tilt. We note that Eq. (4) is a dimensionless number which depends on the tilt v_t/v_F but is independent of v_F for a given tilt. Recently it was shown that for a single node with negligible tilt, the trace of the response (i.e. $\sum_{P_A=\{x,y,z\}} \bar{J}_{i=P_A}$ where P_A is the Poyting vector) is universal and proportional to the chirality [31]. It is easy to see that this result survives for finite tilt over a limited range of chemical potential.

For Weyl semimetals, it is possible to break both TR and I symmetries. In these cases, each Weyl node can

have different parameter values and chemical potentials. $\bar{\mathrm{J}}$ coming from different nodes are not symmetry-related and there is no current cancelation. Only when there is I symmetry, as we show below, will the photocurrents lead to cancelation.

Symmetry consideration.—In centrosymmetric Weyl semimetals, a Weyl node at $\vec{k}$ is related to another one at $-\vec{k}$ about the inversion center (IC) [Fig. 2(a)]. Their Hamiltonians take the same form as Eq. (1) with the relations $\mathrm{q_i} \leftrightarrow -\mathrm{q_i}$ and $\sigma_\mathrm{j} \leftrightarrow \sigma'_\mathrm{j} = \mathrm{P}\sigma_\mathrm{j}\mathrm{P}^{-1}$. The inversion P just changes the basis of σ_j. Hence, I-related nodes have opposite tilt and opposite chirality. Similarly, with TR symmetry, two Weyl nodes are related about the time-reversal invariant momentum (TRIM) with the relations $\mathrm{q_i} \leftrightarrow -\mathrm{q_i}$ and $\sigma_\mathrm{j} \leftrightarrow -\sigma''_\mathrm{j} = \mathrm{T}\sigma_\mathrm{j}\mathrm{T}^{-1}$, where T is the TR transformation. Thus, two TR-related nodes have opposite tilt but the same chirality [Fig. 2(b)]. Even though each monopole has to be accompanied by an anti-monopole, there is no symmetry restriction between them.

Importantly, the photocurrent depends on the sign of the tilt and the chirality. According to the response function [Eq. (4)], when we change $\mathrm{v_t} \to -\mathrm{v_t}$ and $\hat{\mathrm{v}}_{\mathrm{i,j}} \to -\hat{\mathrm{v}}_{\mathrm{i,j}}$, it is equivalent to $\vec{q} \to -\vec{q}$ and the integral yields $\bar{J}_i \to -\bar{J}_i$. With this relation, we can decompose the photocurrent from the n-th Weyl node as

$$\vec{J}^{(n)}(\mathrm{sgn}[v_t^{(n)}], \chi^{(n)}) = \mathrm{sgn}[v_t^{(n)}]\vec{J}_0^{(n)} + \chi^{(n)}\vec{J}_\chi^{(n)}. \quad (5)$$

This is because the other two components (one is proportional to $\mathrm{sgn}[\mathrm{v_t^{(n)}}] \times \chi^{(\mathrm{n})}$ and the other is independent on any of them) have to sum to zero. In. Eq. (5), the first component changes sign for opposite tilts and can be generated by a linearly polarized drive, whereas the second chirality-dependent term can only be induced by a circularly polarized light.

Mirror symmetry is common in realistic Weyl materials. A mirror reflection flips the sign of the Weyl momentum along the mirror axis and relates a monopole to an anti-monopole. However, it does not lead to cancelation of photocurrent because the drive breaks the mirror symmetry of the photocurrent response.

With these symmetry considerations, we conclude that the overall photocurrent has to balance out when there is I symmetry. For noncentrosymmetric systems with TR symmetry, a minimal number of two pairs of Weyl nodes can produce a non-zero response $2(\vec{J}_\chi - \vec{J}'_\chi)$. The photocurrent relations are graphically summarized in Fig. 2(a-b). In a Weyl system without any symmetry, both $\vec{J}_0$ and $\vec{J}_\chi$ can survive. Note that the non-zero photocurrent originates from the different tilts and anisotropies between monopoles and anti-monopoles. While any chemical potential difference can help in a similar way, we shall only consider identical chemical potentials for each Weyl node for the rest of the paper.

Photocurrent by monochromatic drives.—We explore various dependences of photocurrents in noncentrosymmetric Weyl semimetals with TR symmetry due to a circularly polarized drive. For illustrative purpose, we consider a minimal setup of four Weyl nodes, where two monopoles are tilted along $\mathrm{q_z}$ with opposite tilt velocities $\mathrm{v_t}$ and $-\mathrm{v_t}$, while the anti-monopole dispersions are upright. The photon propagates along the $\mathrm{q_x} - \mathrm{q_z}$ plane and is parameterized as $\vec{A}(t) = A\,(\cos\theta_A \cos\omega t, \xi \sin\omega t, -\sin\theta_A \sin\omega t)$ with $\xi = \pm 1$ controlling the polarization. Below, we consider the isotropic limit, i.e. $\hat{v}_{i,j} = \delta_{i,j}$.

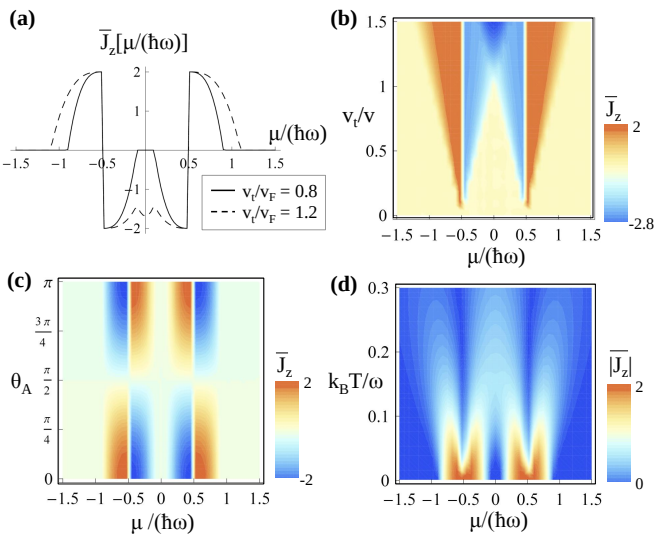

FIG. 3. Demonstrations of photocurrents in a noncentrosymmetric Weyl semimetal driven by a monochromatic circularly polarized light of frequency ω. Two pairs of isotropic Weyl nodes are considered with tilt velocities $\mathrm{v_t}$, $-\mathrm{v_t}$, 0 and 0. The tilts are along $\hat{z}$ and the light propagates at an angle θ_A from $\hat{\mathrm{z}}$. $\bar{\mathrm{J}}$ gives the dimensionless current. (a) Photocurrent at $\mathrm{T} = 0$ and $\theta_\mathrm{A} = 0.3$. With a type-I tilt (i.e. $|\mathrm{v_t}| < \mathrm{v_F}$), $\bar{\mathrm{J}}_\mathrm{z}$ is non-zero when the chemical potential μ falls in the region that supports asymmetric transitions. The sharp change of $\bar{\mathrm{J}}_\mathrm{z}$ at $|\mu|/(\hbar\omega) = 0.5$ is caused by the fact that the two nodes without tilt can no longer be excited when $|\mu| > \hbar\omega/2$. When the tilt is of type-II ($|\mathrm{v_t}| > \mathrm{v_F}$), $\bar{\mathrm{J}}_\mathrm{z}$ does not vanish even at $\mu = 0$. (b) $\bar{\mathrm{J}}_\mathrm{z}$ as a function of the tilt $\mathrm{v_t/v_F}$ and μ at $\mathrm{T} = 0$ and $\theta_\mathrm{A} = 0.3$. The region of non-zero $\bar{\mathrm{J}}_\mathrm{z}$ increases with the tilt of the Weyl spectra. (c) $\bar{\mathrm{J}}_\mathrm{z}$ as we vary θ_A at $\mathrm{T} = 0$ and $\mathrm{v_t/v_F} = 0.8$. The flow of the photocurrent follows the light propagation. (d) Temperature dependence of $|\bar{\mathrm{J}}_\mathrm{z}|$ at $\mathrm{v_t/v_F} = 0.8$ and $\theta_\mathrm{A} = 0.3$. For $\hbar\omega \sim 120$ meV and at room temperature ($\mathrm{k_BT}/(\hbar\omega) \sim 0.22$), 1/4 of the value still remains.

Figure 3(a) plots the dimensionless photocurrent response $\bar{\mathrm{J}}_\mathrm{z}$ at zero temperature with $\theta_A = 0.3$ and finite tilts. When $0 < \mathrm{v_t/v_F} < 1$, the signal is non-zero due to asymmetric excitations assisted by the tilt [Fig. 1(c)]. When $|\mu| < |-\mathrm{v_t/v_F} + 1|\,\hbar\omega/2$, the Weyl nodes are symmetrically excited and the chiral photocurrents from the monopoles and the anti-monopoles carry the same magnitudes but opposite directions. As $|\mu|$

is increased, the magnitudes of both currents decrease in a tilt-dependent manner, resulting in an imbalanced photocurrent $2[\vec{J}_\chi(\mu/\omega) - \vec{J}'_\chi(\mu/\omega)]$. When $|\mu|$ exceeds $|v_t/v_F + 1|\,\hbar\omega/2$, vertical transitions are no longer allowed and every current vanishes. Note that the sharp jump of $\bar{J}_z$ at $|\mu| = \hbar\omega/2$ happens because we consider the special case of two untilted Weyl cones and is not a generic feature.

The region for non-vanishing current can be expanded by increasing the tilt. In the type-II Weyl phase with $|v_t| > v_F$, we have $\bar{J}_z \neq 0$ as long as $|\mu| < |v_t/v_F + 1|\,\hbar\omega/2$. Interestingly, the photocurrent survives at $\mu = 0$. The reason is that in the type-II regime, the photoexcitation depends strongly on the direction $\hat{q}$ and thus is anisotropic even at the neutrality point. Figure 3(b) presents the tilt and chemical potential dependences for the photocurrent. It provides an idea of the working requirements for the photovoltaic effect. $\bar{J}$ is of order one and its sign is controlled by the light polarization. In the isotropic limit, the photocurrent and the Poynting vector of the drive share the same direction as shown in Fig. 3(c).

In order to investigate the possibility for room temperature photocurrent generation, we plot the temperature dependence of $|\bar{J}_z|$ in Fig. 3(d). Our results indicate that a sizeable portion of the photocurrent survives with $k_BT \simeq 0.2\ \hbar\omega$. For an IR radiation with $\hbar\omega \sim 120$ meV and room temperature $k_BT = 26$ meV, $\bar{J}$ remains a quarter of its zero-temperature value.

We provide an estimation of the photocurrent density driven by a CW CO_2 laser. For IR detection applications, we consider $\hbar\omega \sim 120$ meV, and a typical laser intensity $I = \epsilon_0 c(\hbar\omega A/e)^2 \sim 10^6$ Wm^{-2} [8]. At low temperature, the measured $\tau \sim 45$ ps, corresponding to a long mean free path ($\sim 5\ \mu$m) [32]. At room temperature, τ can be reduced by 50 as inferred from resistivity measurements [32]. Such a large τ implies a weak disorder effect in Weyl semimetals. We estimate a large $|J| \sim 4.3 \times 10^7$ Am^{-2} at low temperature. We remark that this result does not require any μ imbalance. Instead, finite tilts and μ are necessary.

Material candidates to probe this photovoltaic effect include the type-I TaAs family [33–36], or the type-II compounds such as WTe_2 [15] and $MoTe_2$ [37]. For type-I materials with small tilts, one would require $\hbar\omega \sim 2\mu$. With a finite tilt, for instance $SrSi_2$ [38] that has $v_t/v_F \sim 0.6$ and $\mu \sim 22$ meV, one can have a detection window of wavelength $\sim 10 - 50\ \mu$m. The operational window becomes even larger for type-II Weyl semimetals according to Fig. 3(b).

A film geometry is required to avoid any absorption issue. For a system of thickness L_z and area L_xL_y with four Weyl nodes, the number of photons being absorbed ($4L_xL_yL_z\sum_q[n_+(\tilde{q}) - n^0_+(\tilde{q})]$) and the number of photons from the drive ($I(\omega)L_xL_y\tau/(\hbar\omega)$) provide an estimation of the absorption length scale $L_a \sim 4\pi^2\hbar\epsilon_0 c v_F/(\omega e^2) \sim$ 700 nm. An ideal device shall have $L_z \lesssim L_a$.

We contrast the performance of our effect with other photodetectors using the external quantum efficiency η, defined as the ratio of the number of charge carriers to the number of incident photons [39]. For a Weyl semimetal with $L_z = 100$ nm and a lateral dimension of a few μm, $\eta = \hbar\omega|J|L_z/(eIL_x) \sim 10^{-3} - 10^{-2}$ for mid-infrared frequency (~ 0.1 eV) at room temperature. In comparison, graphene grown on substrates designed to break I symmetry has been under study as photodetector. The corresponding substrates introduce a strong disorder scattering and the existing and optimized photodetector has a very low $\eta \sim 10^{-5}$ [40]. We also emphasize that in comparison with devices based on photoconductivity, in our case the carriers move with a net velocity, giving rise to a current without any background.

Blackbody radiation detections.—Conventional semiconductor-based photodetectors are limited to wavelength less than 4 μm due to finite bandgaps [39]. Even in graphene-based devices, the photodetections are either restricted to the near-infrared regime [41], or suffer from low efficiency [40]. Our proposed effect can overcome these challenges through its wide range of working window. According to Planck's law, a blackbody object at an equilibrium temperature T_b has a continuous spectrum peaked at $\hbar\omega \sim 2.8\ k_BT_b$, corresonding to 73 meV (or 17 μm) at room temperature. By a straightforward generalization of Eq. (3) and (4) for blackbody radiation, one can show that up to $\sim 1/3$ of the dimensionless response survives at room temperature [42], indicating the suitability of Weyl semimetals for IR detections. We remark that broadband quarter-wave plates as circular polarizers exist for both mid-[43] and far-infrared [44, 45] regimes.

Conclusion.—Based on symmetry analyses and perturbative calculations, we predict a significant photocurrent generation in noncentrosymmetric Weyl semimetals. The photovoltaic process is a consequence of broken I symmetry and finite tilts of the dispersions which are unique to Weyl systems. We show that the effect remains significant in a large window of operating parameters, correspondence to temperature, chemical potential, and frequency of the light source. The predicted photocurrent can be readily detected using standard laser experiment techniques and existing Weyl materials. Our findings reveal the suitability for using Weyl semimetals as room temperature IR detectors.

Acknowledgements.— We thank Nuh Gedik for very helpful discussions. P.A.L. acknowledges the support from DOE Grant No. DE-FG02-03-ER46076 and the Simons Fellows Program. G.R. acknowledges the supported from NSF through DMR-1410435. N.H.L. acknowledges supports from I-Core, the Israeli excellence center Circle of Light and from the People Programme (Marie Curie Actions) of the European Union's Seventh Framework under REA Grant Agreement No. 631696.

P.A.L. and C.-K.C. thank the hospitality of the CMT group at Caltech where this work was carried out. G.R. thanks the Aspen Center for Physics where a part of the work was done.

[1] M. Z. Hasan and C. L. Kane, Rev. Mod. Phys. **82**, 3045 (2010).
[2] X.-L. Qi and S.-C. Zhang, Rev. Mod. Phys. **83**, 1057 (2011).
[3] A. H. Castro Neto, F. Guinea, N. M. R. Peres, K. S. Novoselov, and A. K. Geim, Rev. Mod. Phys. **81**, 109 (2009).
[4] P. Hosur, Phys. Rev. B **83**, 035309 (2011).
[5] A. Junck, G. Refael, and F. von Oppen, Phys. Rev. B **88**, 075144 (2013).
[6] N. H. Lindner, A. Farrell, E. Lustig, G. Refael, and F. von Oppen, arXiv:1403.0010.
[7] A. Abanov, V. L. Pokrovsky, W. M. Saslow, and P. Zhou, Phys. Rev. B **85**, 085311 (2012).
[8] J. W. McIver, D. Hsieh, H. Steinberg, P. Jarillo-Herrero, and N. Gedik, Nat Nano **7**, 96 (2012).
[9] Y. B. Lyanda-Geller, S. Li, and A. V. Andreev, Phys. Rev. B **92**, 241406 (2015).
[10] T. Morimoto and N. Nagaosa, Phys. Rev. B **93**, 125125 (2016).
[11] K. W. Kim, T. Morimoto, and N. Nagaosa, arXiv:1607.03888.
[12] K. Kuroda, J. Reimann, J. Güdde, and U. Höfer, Phys. Rev. Lett. **116**, 076801 (2016).
[13] K. N. Okada, N. Ogawa, R. Yoshimi, A. Tsukazaki, K. S. Takahashi, M. Kawasaki, and Y. Tokura, Phys. Rev. B **93**, 081403 (2016).
[14] M. Trescher, B. Sbierski, P. W. Brouwer, and E. J. Bergholtz, Phys. Rev. B **91**, 115135 (2015).
[15] A. A. Soluyanov, D. Gresch, Z. Wang, Q. Wu, M. Troyer, X. Dai, and B. A. Bernevig, Nature **527**, 495 (2015).
[16] S. Zhong, J. E. Moore, and I. Souza, Phys. Rev. Lett. **116**, 077201 (2016).
[17] S. Zhong, J. Orenstein, and J. E. Moore, Phys. Rev. Lett. **115**, 117403 (2015).
[18] K. Taguchi, T. Imaeda, M. Sato, and Y. Tanaka, Phys. Rev. B **93**, 201202 (2016).
[19] C.-K. Chan, P. A. Lee, K. S. Burch, J. H. Han, and Y. Ran, Phys. Rev. Lett. **116**, 026805 (2016).
[20] H. Ishizuka, T. Hayata, M. Ueda, and N. Nagaosa, arXiv:1607.06537.
[21] L. Wu, S. Patankar, T. Morimoto, N. L. Nair, E. Thewalt, A. Little, J. G. Analytis, J. E. Moore, and J. Orenstein, arXiv:1609.04894.
[22] S. D. Ganichev, S. N. Danilov, V. Bel'kovc, E. L. Ivchenko, H. Ketterla, L. E. Vorobjev, M. Bichlerd, W. Wegscheider, and W. Prettl, Physica E **10**, 52 (2001).
[23] E. L. Ivchenko and G. E. Pikus, *Superlattices and Other Heterostructures: Symmetry and Optical Phenomena*, 2nd ed. (Springer Series in Solid-State Sciences, 1997) chapter 10.5.
[24] O. Vafek and A. Vishwanath, Annual Review of Condensed Matter Physics **5**, 83 (2014).
[25] A. A. Burkov, Journal of Physics: Condensed Matter **27**, 113201 (2015).
[26] T. Morimoto and N. Nagaosa, (2016), arXiv:1605.05409.
[27] J. Hu, J. Y. Liu, D. Graf, S. M. A. Radmanesh, D. J. Adams, A. Chuang, Y. Wang, I. Chiorescu, J. Wei, L. Spinu, and Z. Q. Mao, Scientific Reports **6**, 18674 EP (2016).
[28] S. Jeon, B. B. Zhou, A. Gyenis, B. E. Feldman, I. Kimchi, A. C. Potter, Q. D. Gibson, R. J. Cava, A. Vishwanath, and A. Yazdani, Nat Mater **13**, 851 (2014).
[29] A. A. Burkov, M. D. Hook, and L. Balents, Phys. Rev. B **84**, 235126 (2011).
[30] P. Hosur, S. A. Parameswaran, and A. Vishwanath, Phys. Rev. Lett. **108**, 046602 (2012).
[31] F. de Juan, A. G. Grushin, T. Morimoto, and J. E. Moore, arXiv:1611.05887.
[32] C. Zhang, Z. Yuan, S. Xu, Z. Lin, B. Tong, M. Zahid Hasan, J. Wang, C. Zhang, and S. Jia, (2015), arXiv:1502.00251.
[33] S.-M. Huang, S.-Y. Xu, I. Belopolski, C.-C. Lee, G. Chang, B. Wang, N. Alidoust, G. Bian, M. Neupane, C. Zhang, S. Jia, A. Bansil, H. Lin, and M. Z. Hasan, Nat Commun **6** (2015).
[34] H. Weng, C. Fang, Z. Fang, B. A. Bernevig, and X. Dai, Phys. Rev. X **5**, 011029 (2015).
[35] S.-Y. Xu, I. Belopolski, N. Alidoust, M. Neupane, G. Bian, C. Zhang, R. Sankar, G. Chang, Z. Yuan, C.-C. Lee, S.-M. Huang, H. Zheng, J. Ma, D. S. Sanchez, B. Wang, A. Bansil, F. Chou, P. P. Shibayev, H. Lin, S. Jia, and M. Z. Hasan, Science **349**, 613 (2015).
[36] B. Q. Lv, H. M. Weng, B. B. Fu, X. P. Wang, H. Miao, J. Ma, P. Richard, X. C. Huang, L. X. Zhao, G. F. Chen, Z. Fang, X. Dai, T. Qian, and H. Ding, Phys. Rev. X **5**, 031013 (2015).
[37] Z. Wang, D. Gresch, A. A. Soluyanov, W. Xie, S. Kushwaha, X. Dai, M. Troyer, R. J. Cava, and B. A. Bernevig, (2015), arXiv:1511.07440.
[38] S.-M. Huang, S.-Y. Xu, I. Belopolski, C.-C. Lee, G. Chang, T.-R. Chang, B. Wang, N. Alidoust, G. Bian, M. Neupane, D. Sanchez, H. Zheng, H.-T. Jeng, A. Bansil, T. Neupert, H. Lin, and M. Z. Hasan, Proceedings of the National Academy of Sciences **113**, 1180 (2016).
[39] M. Razeghi and B.-M. Nguyen, Reports on Progress in Physics **77**, 082401 (2014).
[40] Z. Zhu, S. Joshi, and G. Moddel, IEEE Journal of Selected Topics in Quantum Electronics **20**, 70 (2014).
[41] F. H. L. Koppens, T. Mueller, P. Avouris, A. C. Ferrari, M. S. Vitiello, and M. Polini, Nat Nano **9**, 780 (2014), review.
[42] See Supplemental Material for the study of photocurrent response due to blackbody radiation.
[43] P. E. Sieber and D. H. Werner, Opt. Express **22**, 32371 (2014).
[44] J.-B. Masson and G. Gallot, Opt. Lett. **31**, 265 (2006).
[45] Z. Chen, Y. Gong, H. Dong, T. Notake, and H. Minamide, Optics Communications **311**, 1 (2013).